Ion size effects on electric double layers and ionic transport through ion-exchange membrane systems

Pierre Magnico

Ion size effects on electric double layers and ionic transport through ion-exchange membrane systems

Pierre Magnico

Laboratoire de Mécanique, Modélisation et Procédés Propres (UMR CNRS 6181), IMT La Jetée, Technopôle de Château-Gombert, 38, Rue Frédéric Joliot-Curie, Marseille, France

The density function theory is used to study the density profiles and the transport properties of an ion-exchange membrane system submitted to an electric potential drop. As the ionic density increases, hard sphere interaction between ions becomes dominant and the ion size must be taken into account. The results show that the density distribution and the transport properties depend on the bulk electrolyte density. At equilibrium the charge inside the electric double layer (EDL) adjacent to the membrane decreases and the membrane electric potential increases as the bulk density increases. For high bulk density of unsymmetric electrolyte, secondary charge layers are observed inside the EDL. In the membrane the anion-density-to-bulk-density ratio increases when the bulk density increases from small to moderate values owing to the membrane potential increase. But it decreases abruptly at high bulk density values owing to the increase of the non-ideal electrostatic interaction. At a given electric potential drop, the current/voltage curves follow the variation of this ratio with respect to the bulk density at equilibrium. As the current density approaches the limiting one, the amplitude of the secondary charge layers decreases and the EDL thickness increases.

1. Introduction

The Nernst–Planck (NP) equation is commonly used to model the ion transport through industrial membrane systems. However the NP equation includes several approximations such as proportionality between the ion velocity and the thermodynamic forces, absence of cross-linking between ions, no definition of the diffusion coefficient, ions approximated to point charges [1]. In order to take into account of the complexity of the physico-chemical properties of industrial membrane systems, the NP equation has been extended by introducing ion/solvent and ion/membrane interactions (e.g. ion pairing, dielectric saturation, dielectric exclusion [2–4]). However, to my knowledge and contrary to the biological engineering, only few investigations about the ion size effects on the ion transport through membrane systems or micro- and nanochannels have been carried out in chemical engineering [5–16].

In order to take into account of these effects, several theoretical models based on the thermodynamic statistics have been used to investigate the structure of electrolytes in equilibrium with a charged surface. These studies have shown that even at moderate density, the electric double layer (EDL) is strongly modified by the presence of charge layers which cannot be modelled by the Poisson–Bolzmann (PB) equation. This perturbated EDL induces a modification of the selectivity and of the electrophoretic properties revealing that pair correlation and volume exclusion must be taken into account [17–20].

The goal of the present work is to study the effect of the ion size on the spatial distribution of density and on the properties of the ion transport through membrane systems. This investigation has been carried out by means of the density functional theory (DFT). The DFT is an integral equation theory which determines the thermodynamic properties of an inhomogeneous fluid. It is based on the functional minimisation of the grand canonical potential [21,22]. DFT has been applied successfully to interfacial and phase behaviour in a wide variety of systems, such as colloidal fluids, polymeric fluids, liquid crystals and biological systems [20,23,24]. In this work the membrane system consists in a one-dimensional charged membrane immersed in a bulk electrolyte solution and separating two baths. This simplistic system, commonly used to model electrochemical systems [25–28], does not take account of the membrane pore structure and of the radial ion distribution in the pore. The use of the homogeneous model (i.e. the Toerell–Meyer–Sievers model) instead of the three dimensional space charge model [4,5,13,29,30] is justified if the screening length associated with the membrane charge density is greater than half the pore radius [31,32]. However the aim of the paper is to analyse the perturbation of the EDL adjacent to the

* Tel.: +33 4 91 05 43 56; fax: +33 4 91 11 85 02.
E-mail address: magnico@l3m.univ-mrs.fr

membrane/bath interface induced by the introduction of the ion size and to evaluate the induced modification of the transport properties, even if the membrane charge density ranges up to 10 M. In this analysis, the DFT results are compared to the ones computed with the classical Poisson–Nernst–Planck (PNP) equation set over a large range of electrolyte density and of membrane charge.

In this paper the membrane system, the modified PNP equation set and the numerical method are first described (the DFT applied to ionic fluid is presented in Appendix A). In the next section the density, the electric potential and the charge profiles are analysed in a membrane system at equilibrium in the case of an unsymmetric elecrolyte ($CaCl_2$). Results obtained with a symmetric one (NaCl) are reported in Appendix B. Finally, the transport properties of the membrane system under an electric potential drop are studied for the two electrolytes. Profiles of concentration, of electric potential and of charge are described in Appendix C.

2. Membrane system and numerical methodology

2.1. Description of the membrane system

The membrane system consists in a negative charged membrane of length L embedded in a binary electrolyte solution the density of which is ρ_o. The two baths on both sides of the membrane have a length δ. So the membrane system length is $L+2\delta$ [27]. Along the membrane the fixed charge density Y is constant. We assume that the membrane and the ions do not interact chemically. The diffusion coefficient D_i and the dielectric constant ε are constant over all the membrane system. However, owing to the high values of ρ_o and of Y used in this work, the dependence of these coefficients with respect to the local ion density would have to be taken into account [10,33,34].

2.2. One-dimensional ion transport

Steady-state ion transport under concentration gradient and external field is defined by the divergence free of the flux of each species:

$$\frac{\partial}{\partial x}J_i = 0 \tag{1}$$

In the case of small thermodynamic forces the flux are linearly dependent on these forces, and the following one-dimensional phenomenological relation is applied:

$$J_i = -\frac{D_i\rho_i(x)}{kT}\frac{\partial\mu_i}{\partial x} \tag{2}$$

where μ_i is the chemical potential defined at equilibrium, $\rho_i(x)$ the density of the species i located at x, k the Boltzmann constant, T the absolute temperature. Eq. (2) means that a system out of thermodynamic equilibrium may be approximated to a system at local equilibrium defined by a chemical potential varying spatially. The DFT is used to derive the expression of μ_i. The extension of the Nernst–Planck (NP) equation to high concentration lies in additional terms in the chemical potential expression: a hard sphere contribution μ_i^{hs} and an electrostatic one μ_i^{es}. The ions are assimilated to charged hard sphere. μ_i^{hs} represents the excluded volume effect of uncharged spherical particles and μ_i^{es} represents the ion size effect on the screening efficiency of the electrical double layer located around each ion. The sum of the two contributions is equivalent to the logarithm of the activity coefficient of the electrolyte. These two contributions depend on the density of all the ionic species. Therefore all the NP equations are coupled via μ_i^{es} and μ_i^{hs}. In the following, the term 'ideal' represents the classical NP approach in which the excess terms μ_i^{es} and μ_i^{hs} are omitted in the opposite of the 'non-ideal' term. Attempts to justify the use of the DFT (named in this case dynamic density functional theory—DDFT) in nonequilibrium situations have been carried out by means of the stochastic equations of motion for colloidal fluids or by means of the Newton one for atomic fluid. The main assumptions are that the equilibrium is local and that the gradient of the chemical potential computed at equilibrium is a thermodynamic force. Comparison with Monte Carlo simulations has proved that the DDFT is accurate enough [35–37]. Here DDFT is replaced by DFT because the simulations in nonequilibrium regime are carried out at steady-state.

In the figures, the ideal curves represent the results of the computations carried out without these excess terms. Therefore these curves represent the results of computation with the classical PNP equations. The detail of the computation of μ_i is given in [38,39] and is briefly presented in Appendix A.

The adimensionalized PNP/DFT equation set has the following expression:

$$\frac{\partial}{\partial x}\left(D_i\rho_i(x)\frac{\partial\mu_i}{\partial x}\right) = 0 \tag{3}$$

$$2\chi I\frac{\partial^2}{\partial x^2}\Phi(x) = -\sum_i z_i\rho_i(x') + Y(x) \tag{4}$$

With

$$\mu_i(x) = Ln(\rho_i(x)) + z_i\chi\Phi(x) + \mu_i^{hs}(x) + \mu_i^{es}(x) \tag{5}$$

$$\chi = \frac{e|\Phi_d|}{kT} \tag{6}$$

$$I = \frac{1}{2}\sum_i \rho_{oi}z_i^2 \tag{7}$$

$$Y(x) = Y \quad \text{if } 0 < x < L \tag{8}$$

$$Y(x) = 0 \quad \text{elsewhere}$$

where e the elementary charge, Φ_d the Donnan potential, ρ_{oi}.the density of the species i at $x=-\delta$. In Eq. (5), $\mu_i^{hs}(x)$ and $\mu_i^{es}(x)$ are defined in Appendix A.

In Eqs. (3)–(5) and (7), all the variable are used in the reduced form: the lengths, the fixed charge and ion densities, the diffusion coefficients, the electric potential and the chemical potential are normalised by the Debye length λ_d, a reference salt density ρ_o^{ref}, the mean diffusion coefficient ($\overline{D}$), the Donnan potential $|\Phi_d|$ and the thermal energy kT respectively. The mean diffusion coefficient and the Debye length have the following expression:

$$\overline{D} = \frac{\sum_i \rho_{oi}D_i}{\sum_i \rho_{oi}} \tag{9}$$

$$\lambda_d = \left(\frac{\varepsilon kT}{e^2}\frac{1}{2\rho_{scale}I}\right)^{1/2} \tag{10}$$

With $\rho_{scale} = 10^3\mathcal{N}_a\rho_o^{ref}$ where $\mathcal{N}_a$ is the Avogadro number. The quantity ρ_{scale} is used because in the definition of λ_d and in the dimensionalized PNP equation set the unit of the density ρ_i is m^{-3} and the unit of ρ_o^{ref} is Mole/L. The current density is normalised by $I_{ref} = e\overline{D}\rho_{scale}/\lambda_d$ and has the following expression $I_C = \sum_i z_i J_i$.

2.3. Resolution of the transport equation set

In Eqs. (3) and (4), the variables are μ_i, ρ_i, Φ. In order to lower the complexity of the problem, the weighted function $n_\alpha(x)$, defined in Appendix A and in [38], is considered as an additional

explicit variable. So Eq. (A.6) is the fourth equation of the transport equation set.

The two differential equations are discretized by means of the finite difference method. At iteration $n+1$, the densities ρ_i^n, the electric potential Φ^n and $n_\alpha(\rho_i^n)$ are known. $n_\alpha(\rho_i^n)$ is the non-local density determined with the density ρ_i^n computed at iteration n. The chemical potential $\mu_i^{n+1/2}$ is first computed by means of Eq. (3). In a second step ρ_i^{n+1} and n_α are computed by means of the Newton method. In a third step, the Poisson equation (Eq. (4)) is solved in order to compute the electric potential Φ^{n+1} with the density profile$\rho_i^{n+1}(x)$. Finally, $\mu_i(\rho_i^{n+1},\Phi^{n+1})$ and $n_\alpha(\rho_i^{n+1})$ are computed. At this step, the species density in the local reference fluid ρ_i^{ref} and the screen parameter Γ are computed with ρ_i^{n+1} by means of the MSA and of the conditions on the electroneutrality and on the ionic strength [34] (see also Appendix A). This computation must be carried out by an iterative method.

In all the numerical computations, the bulk density and the electric potential are imposed at the boundaries located at $x=-\delta$ and $x=L+\delta$. The same value of density ρ_{oi} is imposed at these boundaries, the value of the electric potential is zero at $x=-\delta$. The membrane and the baths have a length of 50 and 100 Debye length (λ_d) respectively. The numerical simulations have been carried out with $T=300$ K, $\varepsilon=78.4$, $D_i=10^{-10}$ m^2/s, $R_{Na+}=1$ Å, $R_{Ca^{2+}}=1$ Å, $R_{Cl-}=1.8$ Å and $\rho_o^{ref}=1$ Mole/L. The cation hydration is not taken into account. The spatial grid is identical to the one used in [27]. The grid is affined over 4 Debye lengths on both sides of the two bath/membrane interfaces and is stretched in the other regions. The membrane and the two baths are discretized with 100 nodes and 80 nodes respectively. Numerical simulations carried out with a higher node number have shown that the discretisation is accurate enough.

3. Analysis of the DFT results at equilibrium

3.1. Density and electric potential profiles in the case of an unsymmetric electrolyte

Figs. 1 and 2 display, on both sides of the left bath/membrane interface, the profiles of the density ratios ρ_i/ρ_o, of the electric potential and of the local charge density ratio Q/ρ_o. These profiles are computed with $Y/\rho_o=-10$ and for ρ_o varying from 10^{-4} to 1. Q is defined as the sum of all the charge densities fixed and mobile: $Q/\rho_o=(2\rho_{Ca^{2+}}-\rho_{Cl^-}+Y)/\rho_o$. The profiles are compared to the ones computed with the ideal approximation (i.e. $\mu_i^{hs}(x)=\mu_i^{es}(x)=0$). With the normalisation used in these figures, all the ideal profiles must be identical to the bold curves because the Donnan potential is a function of Y/ρ_o and because the Poisson and the Nernst–Planck equations are linear with respect to the density. Therefore the ideal profiles depend on Y/ρ_o but not on ρ_o. Here the profiles show that the non-ideality induces a dependence on ρ_o owing to the contribution of $\mu_i^{hs}(x)$ and of $\mu_i^{es}(x)$. We have to notice that the profiles show differences with the ideal ones even at $\rho_o=10^{-4}$ where non-ideal effects are small but observable. Inside the membrane, far from the interface, $\rho_{Ca^{2+}}/\rho_o$ and ρ_{Cl^-}/ρ_o increase with ρ_o when $\rho_o<0.1$ and decrease when $\rho_o>0.1$. For the counter-ion, if $\rho_o>0.01$ a local spatial maximum appears the amplitude of which increases with ρ_o. Its location at $x=1.26$ is not sensitive to ρ_o. At high salt density a local minimum also appears, the location at $x=3.37$ seems independent of ρ_o. To this counter-ion local maximum corresponds a co-ion local minimum and conversely, to the counter-ion local minimum corresponds a co-ion local maximum. However, for the co-ion, their position moves to the membrane centre as ρ_o increases. Outside the membrane, the cation profiles display a minimum when $\rho_o\geq 0.1$. Its location is independent of ρ_o. For the anion, a maximum is observable also when $\rho_o\geq 0.1$, but its location moves to the left boundary.

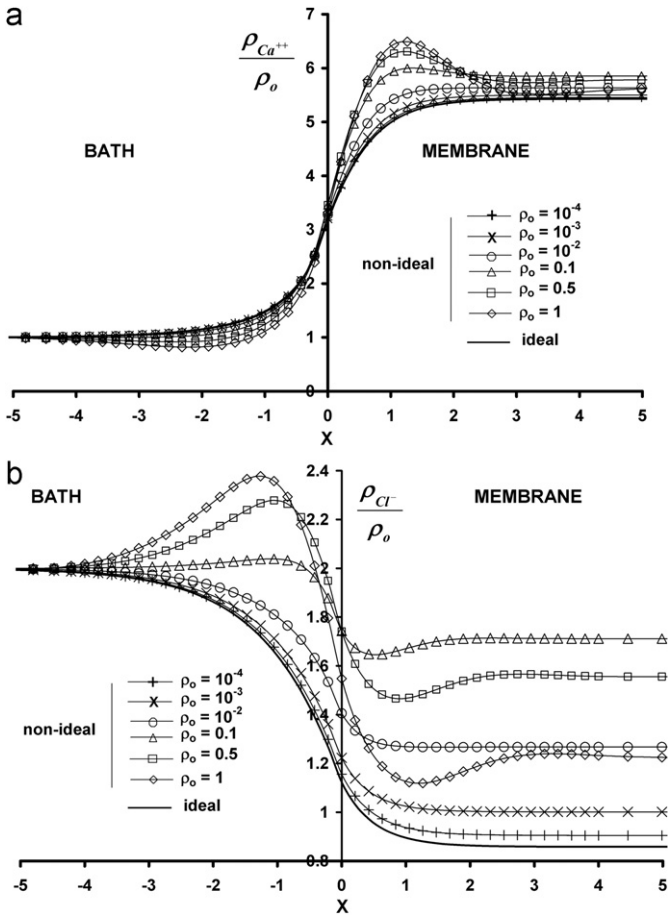

Fig. 1. Electrolyte: $CaCl_2$. Ion density ratio profiles on both sides of the left bath/membrane interface at equilibrium for several salt density values. $Y/\rho_o=-10$.

Qualitative comparisons may be eventually made with MC and DFT computations carried out around a negatively charged plane. In [40], the plane is modelled as a semipermeable membrane. But the membrane is not permeable to all the ions. Its thickness is 0.05 Å. The density profiles displayed in [40] which are related to simulations shown in Fig. 1 correspond to simulation 20. In this simulation, the $R_{Cl-}=2.13$ Å, $R_{Ca^{2+}}=1$ Å, $\rho_o=0.5$ M, the surface charge $\sigma=-0.5$ C m^{-2}. The co-ion profile displays one maximum located at $2R_{Cl-}$, the amplitude of which is $2\rho_{ocl-}$. In Fig. 1, the maximum outside the membrane is located at $1.3R_{Cl-}$ if $\rho_o=0.5$ M and at $1.1R_{Cl-}$ if $\rho_o=1$ M from the left membrane/bath interface. For the counter-ion density profile, the figure in [40] does not allow to verify if it has an extrema. Computation with NaCl 1 M and $\sigma=-0.5$ C m^{-2} (simulation 19) does not display any layering. This confirms the small ion size effects on the density and potential profiles reported in Appendix B.

In the EDL the co-ions move from the membrane to the baths and the counter-ions move in the opposite direction replacing the anions as ρ_o increases. At the same time, successive anionic and cationic secondary layers appear in the EDL. This layering on both sides of the interface induces a secondary layer of negative charge density Q outside the membrane, a positive and a negative secondary charge density layer inside the membrane. The positions of these extrema are independent of ρ_o and correspond to the positions of the cation density extrema. The whole charge ratio in the EDL in the bath side (i.e. $\int_{-\delta}^{0} Q(x)/\rho_o\,dx$) decreases and increases in the membrane side as ρ_o increases owing to the

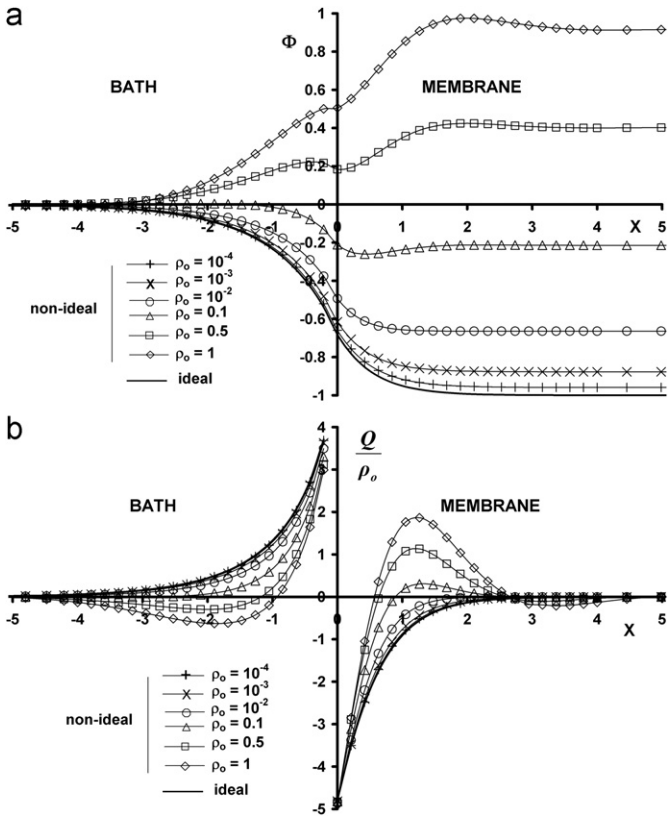

Fig. 2. Electrolyte: $CaCl_2$. Electric potential and charge profiles on both sides of the left bath/membrane interface at equilibrium for several salt density values. $Y/\rho_o = -10$.

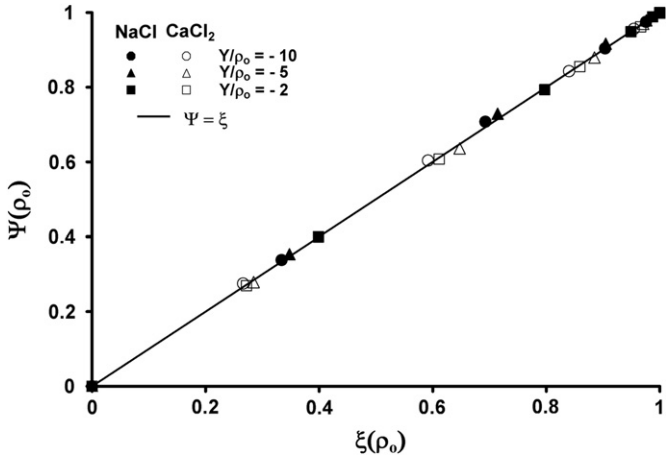

Fig. 3. $\Psi(\rho_o)$ vs. $\xi(\rho_o)$ for ρ_o ranging from 10^{-4} to 1 and $Y/\rho_o = -2$, -5 and -10.

electroneutrality condition over the computational domain. It changes of sign on both sides if $\rho_o > 0.5$. The electric potential increases monotonously as the whole charge ratio in the inner EDL increases. As long as secondary layers do not appear in the outer EDL, i.e. $\rho_o < 0.1$, the electric potential profile keeps the same shape as observed for NaCl (see Appendix B). As soon as these layers appear ($\rho_o > 0.1$), an electric potential inversion is observed. This inversion occurs before the charge inversion.

Fig. 3 displays the correlation between the electric potential at the membrane centre (noted $\Phi_{1/2}$) and the whole charge ratio in the outer EDL (noted $Q_{out} = \int_{-\delta}^{0} Q(x)/\rho_o \, dx$) for $Y/\rho_o = -2$, -5 and -10 and for the two electrolytes. A variable change has been carried out so that the range of variation of Ψ and ξ lies between 0 and 1:

$$\xi(\rho_0) = \frac{Q_{out}(\rho_0) - Q_{out}(\rho_0 = 1)}{Q_{out}(\rho_0 = 10^{-4}) - Q_{out}(\rho_0 = 1)} \tag{11}$$

$$\Psi(\rho_0) = \frac{\Phi_{1/2}(\rho_0) - \Phi_{1/2}(\rho_0 = 1)}{\Phi_{1/2}(\rho_0 = 10^{-4}) - \Phi_{1/2}(\rho_0 = 1)} \tag{12}$$

In this figure, for each value of Y/ρ_o, the curves $\Psi(\rho_0)$ vs. $\xi(\rho_0)$ are close to the straight line $\Psi = \xi$. The dependency of the electric potential with respect to Q_{out} does not depend on EDL structure even if the EDL profile is much modified.

At this step of the description of the EDL structure, it must be observed that the dependence of the extrema position with respect to ρ_o is a consequence of the choice of the characteristic length. In this article, the characteristic length is the Debye length which decreases with the increasing salt density ρ_o. The position of all the extrema moves actually to the interface as ρ_o increases. This means that λ_d is not a relevant characteristic length for the exact location of the extrema but it is relevant for the comparison between profiles with and without non-ideal assumptions because the EDL thickness remains of the order of the Debye length. Moreover, the salt density range of variation is 10^4 and the Debye length one is 10^2.

3.2. Influence of the chemical potential components on the ion partitioning

In order to explain the variation of the density of each species with ρ_o at the membrane centre, the balance between all the components of the individual chemical potential μ_i has been analysed. Figs. 4 and 5 display the difference of all the chemical potential contributions μ_i^ε between the membrane centre ($x = L/2$) and the left boundary ($x = -\delta$) as a function of ρ_o for $Y/\rho_o = -2$, -5 and -10: $\Delta\mu_i^\varepsilon = \mu_i^\varepsilon(x = L/2) - \mu_i^\varepsilon(x = -\delta)$ with $\varepsilon = es$, hs, ρ, ϕ. The ideal component is divided into two terms: the density component ($\mu_i^\rho = Ln(\rho_i)$) and the electric potential one ($\mu_i^\varphi = \Delta\mu_i^\varphi = z_i\chi\Phi$). The sum of the difference of all the components is equal to $\Delta\mu_i = \mu_i(x = L/2) - \mu_i(x = -\delta)$ which must vanish because the system is at equilibrium. As ρ_o decreases from 1 to 0, the non-ideal effects must be less and less important so that as ρ_o approaches 10^{-4}, the curves must converge to values obtained with the ideal approximation. At this step it must be noticed first that the difference of the logarithmic component $\Delta\mu_i^\rho$ is equal to $Ln(\rho_i/\nu_i\rho_o)$, which is equivalent to the logarithm of the ion partitioning. Therefore the curves $\Delta\mu_i^\rho$ vs. ρ_o for $Y/\rho_o = -10$ can be deduced from Fig. 1 at $x = 5$. Second, the electric potential at $x = L/2$ depends on the charge profile in the electric double layer EDL only owing to the electroneutrality condition inside the membrane. In other word, Φ is independent of the electrolyte composition at $x = L/2$.

For the cation (Fig. 4) the hs contribution at $x = L/2$ and at $x = -\delta$ are equal. Therefore the density ratio $\rho_{Ca^{2+}}/\rho_o$ curve (i.e. $\Delta\mu^\rho_{Ca^{2+}}$ curve) is the result of the balance between $\Delta\mu^\varphi_{Ca^{2+}}$ and $\Delta\mu^{es}_{Ca^{2+}}$. $\rho_{Ca^{2+}}/\rho_o$ varies slightly with ρ_o owing to the local electroneutrality condition and to the magnitude of variation of ρ_{Cl^-}/ρ_o with ρ_o. The variation of these two components is monotonous but the rate of variation is noticeable when $\rho_o > 0.01$. It must be recalled that when $\rho_o > 0.1$, $\Phi(L/2)$ changes of sign and the electric potential contribution becomes repulsive. It must be also observed that $\Delta\mu_i^{es}$ does not depend on the density ratio but on the ion density ρ_i itself at $x = -\delta$ and $x = L/2$. In other words it depends on the screening ability of each species at these two locations separately. This explains the variation of $\Delta\mu^{es}_{Ca^{2+}}$ without any noticeable variation of $\Delta\mu^\rho_{Ca^{2+}}$ (i.e. $\rho_{Ca^{2+}}/\rho_o$). Owing to the large charge of cation, $\Delta\mu^{es}_{Ca^{2+}}$ cannot be neglected if $\rho_o > 0.001$

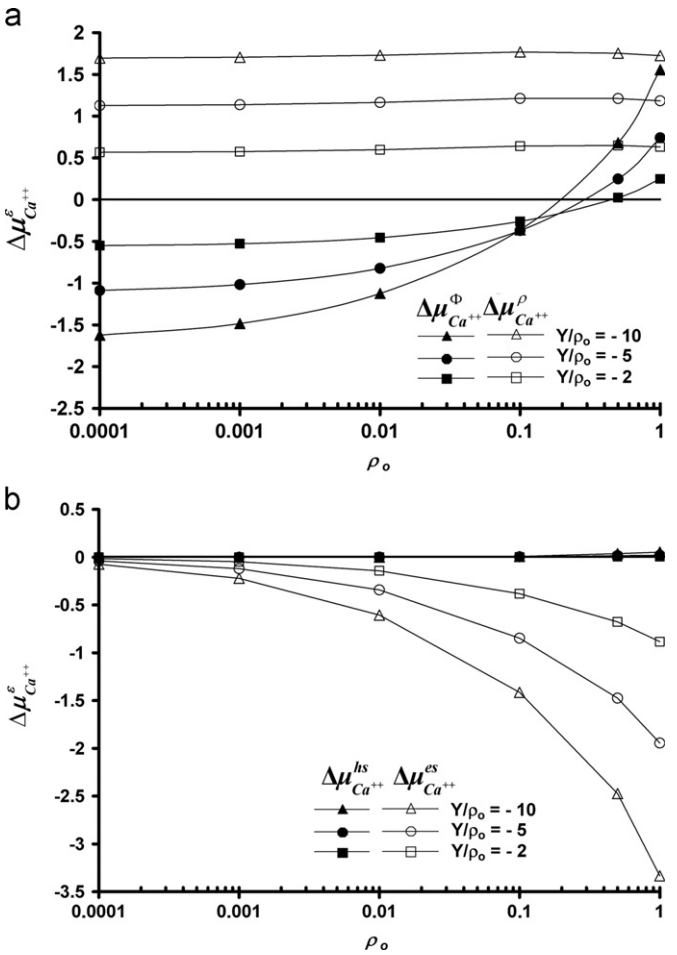

Fig. 4. Electrolyte: $CaCl_2$. Species: Ca^{2+}. Difference of each chemical potential contribution between the membrane centre and the left boundary vs. the salt density for several values of the membrane charge density ratio Y/ρ_o. (a) Density and electric potential contribution and (b) electrostatic and hard sphere contribution.

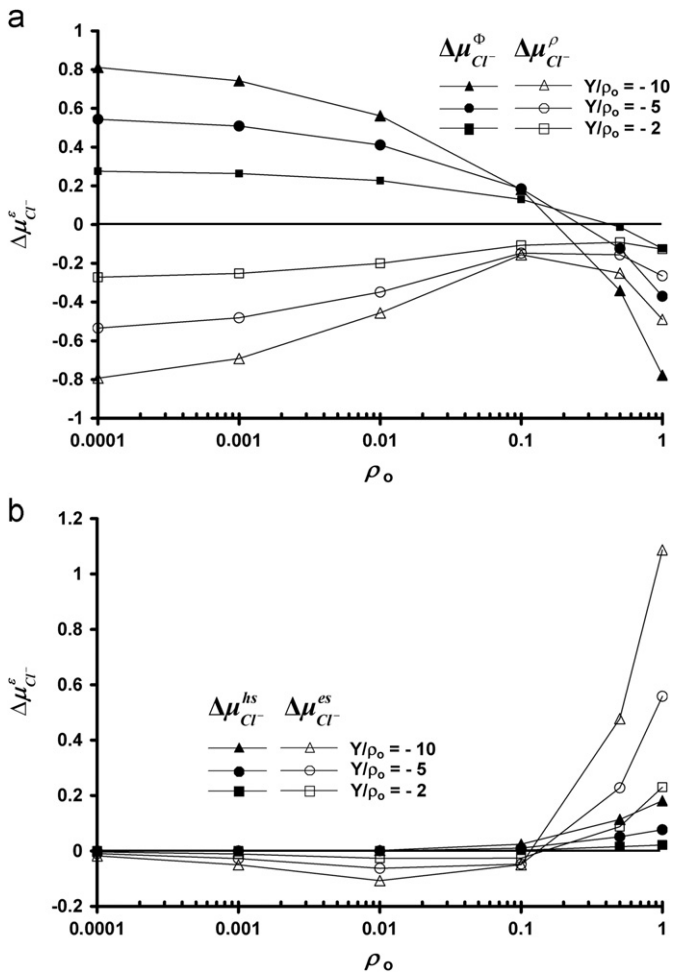

Fig. 5. Electrolyte: $CaCl_2$. Species: Cl^-. Difference of each chemical potential contribution between the membrane centre and the left boundary vs. the salt density for several values of the membrane charge density ratio Y/ρ_o. (a) Density and electric potential contribution and (b) electrostatic and hard sphere contribution.

and its amplitude of variation with ρ_o is much higher than for Na^+ (see Appendix B). For the co-ion (Fig. 5), two regimes with a crossover at $\rho_o = 0.1$ can be observed. If $\rho_o < 0.1$, $\Delta\mu^{\varphi}_{Cl^-}$ and $\Delta\mu^{\rho}_{Cl^-}$ are dominant. This means that the *es* and the *hs* components inside the membrane and at the left boundary are equal. Therefore the density ratio ρ_{Cl^-}/ρ_o depends on the electrical potential only, i.e. the variation of ρ_{Cl^-}/ρ_o does not result from non-ideal effects at $x = L/2$ but from non-ideal effects on the charge distribution in the EDL. When $\rho_o > 0.1$, $\Delta\mu^{es}_{Cl^-}$ is the dominant term. The small repulsive contribution of $\Delta\mu^{hs}_{Cl^-}$ amplifies the decrease of the density ratio.

Simulations carried out with values of Y/ρ_o equal to -2 and -5 show similar behaviour. The value of the salt density threshold is independent of Y/ρ_o. However the amplitude of variation of $\Delta\mu^{\varepsilon}_i$ with ρ_o decreases with Y/ρ_o. As Y/ρ_o decreases, the electrolyte composition approaches the composition at the left boundary and the density decreases inducing less non-ideal effects.

4. Analysis of the current/voltage curves in negatively charged membrane system

In this section the current/voltage curves when a potential drop $\Delta\Phi$ is imposed at the computational domain boundaries are described. The investigation has been carried out in underlimiting current regime, so as the thickness of the EDL is much smaller than the bath one. In Fig. 6, I_{LO} is the limiting current density of a perfectly permselective membrane, i.e. through which the co-ion flux is null [27,28,41,42]. If the excess contribution of the chemical potential is not taken into account:

$$I_{LO} = \frac{(z_1 - z_2) D_1 \nu_2 \rho_o}{\delta} \tag{13}$$

where ν_2 is the stoichiometric number of species 2 for a binary electrolyte ($\nu_1 z_1 = -\nu_2 z_2$). It is convenient to use the ratio I_C/I_{LO} for two reasons. First a simple model gives an expression of I_L as a function of I_{LO}. Second, in the ideal case, the current density is linear with respect to the electrolyte density and depends on the ratio Y/ρ_o. Therefore I_C/I_{LO} is dependent of Y/ρ_o only as Φ_d and χ. So in Fig. 6b one ideal current/voltage curve only is needed for each electrolyte.

Fig. 6a shows the current/voltage curves for NaCl and $CaCl_2$ with $\rho_o = 1$, $Y/\rho_o = -2$, -5 and -10. It must be noted that the current density is multiplied by 2.5 in the case of NaCl because it ranges from 0 to 1.5. In order to carry out a qualitative analysis, the results obtained at equilibrium will be used. Fig. C1b (Appendix C) shows that inside the membrane the density ratio profiles revolve around the equilibrium value without changing the value of the spatial averaged density as the electric potential drop increases. However the density ratio value at equilibrium will not give enough information for the analysis of the current/voltage curve. The value of the anion density ratio at the

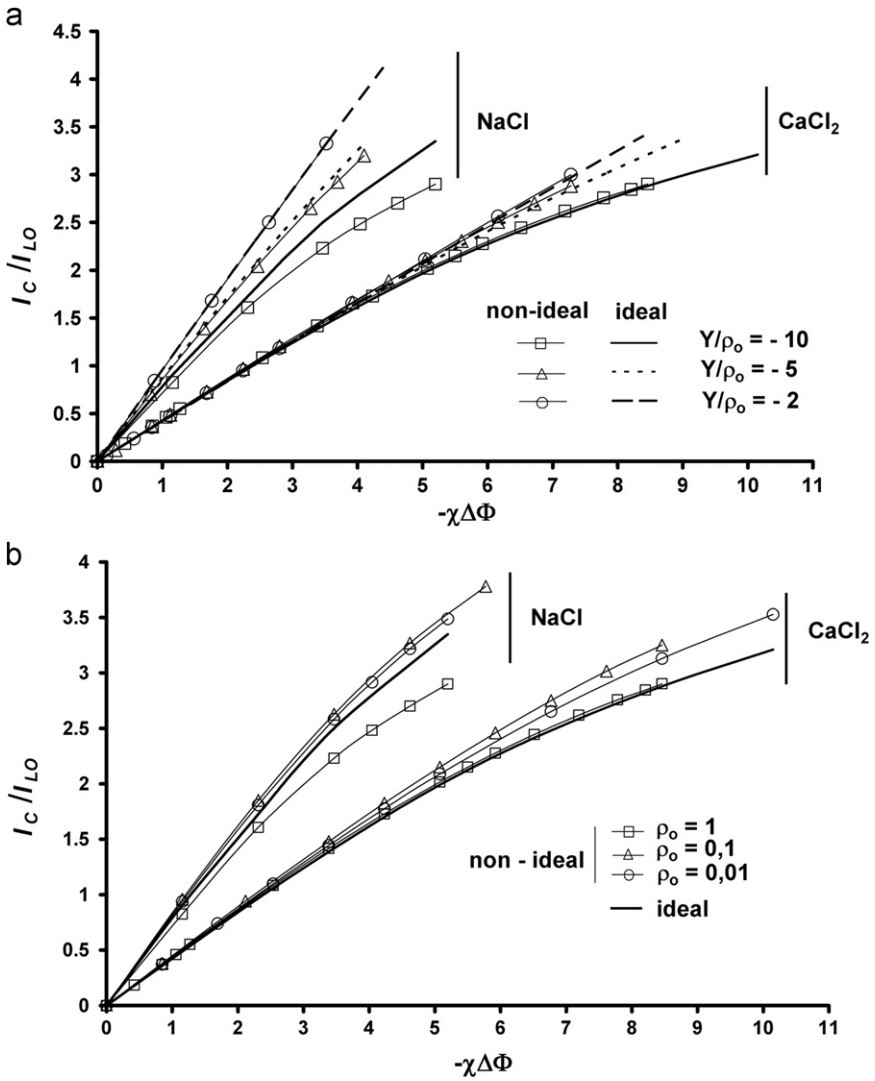

Fig. 6. Current/voltage curves for NaCl and $CaCl_2$: (a) $\rho_o=1$, $Y/\rho_o=-2$, -5, -10; (b) $\rho_o=0.01$, 0.1, 1 and $Y/\rho_o=-10$. For NaCl the value of the current density is multiplied by 2.5.

minimum located in the membrane near the left membrane/bath interface will be also used.

The NaCl curves are analysed first. In the case $Y/\rho_o=-10$ and $\rho_o=1$, a great difference between the ideal curve and the non-ideal one can be observed. Fig. B3a shows that, at the membrane centre, ρ_{Na^+}/ρ_o ($\Delta\mu^{\rho}_{Na^+}$) are equal in the non-ideal case and in the ideal one. On the contrary, Fig. B4a shows that, at the same location, the density ratioρ_{Cl^-}/ρ_o ($\Delta\mu^{\rho}_{Cl^-}$) has a lower value in the non-ideal case than in the ideal one. So the cationic flux should not be sensitive on the ion size effects and the anionic flux should be lower in the non-ideal case. The cationic flux is the main contribution of I_C because the counter-ion density is much greater than the co-ion density. Therefore, in the non-ideal case, I_C should be a little smaller compared to the current density in the ideal case. But, the numerical results have shown that the cationic flux also is smaller in the non-ideal case over all the electric potential drop range investigated and the flux difference increases with $\Delta\Phi$. The explanation is the small value of ρ_{Cl^-}/ρ_o at the minimum located near the left membrane/bath interface. When $\chi\Delta\Phi=-5.2$, this value is 7.5×10^{-3} and 1.6×10^{-2} in the non-ideal case and in the ideal case respectively. These small values are a limiting factor for the density fluxes and a decrease of ρ_{Cl^-}/ρ_o at this minimum at a given value of $\Delta\Phi$ induces a decrease of the cationic flux and amplifies the decrease of I_C.

Fig. 6a shows also that if $Y/\rho_o=-10$ and $\rho_o=1$ the ideal curve is no more linear when $I_C>0.5I_{LO}$. Therefore the value of I_L/I_{LO} is close to unity. In order to make an estimation of I_L, its expression is determined by assuming that at $I_C=I_L$, the co-ion density (ρ_2) is much smaller at the left membrane/bath interface than at the left boundary and that the electroneutrality condition occurs everywhere in the left bath. Using the expression of I_C and of I_{LO}, Eqs. (C.3) and (C.4) at $x=0$ with $Y=0$, we obtain the following expression:

$$I_L=\frac{(z_2J_2/z_1J_1)+1}{(D_2J_2/D_1J_1)+1}I_{LO} \tag{14}$$

The ideal hypothesis and the non-ideal one lead to a value of $1.8I_{LO}$ and of $1.54I_{LO}$ respectively. This estimation does not depend on the value of $\Delta\Phi$ because the flux ratio $J_2/J_1(=J_{Cl^-}/J_{Na^+})$ remains constant over the electric potential drop range. These two values of I_L are coherent with the fact that the non-ideal current/voltage curve is below the ideal one. But this is also surprising because Eq. (14) is obtained with the ideal hypothesis and the flux ratio is computed with the non-ideal one. This coherence is also observed for smaller values of Y/ρ_o.

As Y/ρ_o decreases, at equilibrium ρ_{Cl^-}/ρ_o in the membrane increases (see Fig. B4a). Therefore the value of I_L and the $\Delta\Phi$ range over which the ohmic region takes place must increase as Y/ρ_o

decreases. For example, if $Y/\rho_o = -2$, the value of I_L is equal to $5.4I_{LO}$ and $5.38I_{LO}$ with the ideal and non-ideal hypothesis. These two values are close because, as Y decreases at a given value of ρ_o, the electrolyte composition in the membrane approaches the bulk one. The bulk electrolyte has a lower ion density and the non-ideal contributions have less effects. So the difference between the ideal current/potential curve and the non-ideal one decreases with Y.

For $CaCl_2$, the simulations give very different results. The ideal assumption and the non-ideal one lead to the same results. In the case $Y/\rho_o = -10$, we should have a high discrepancy between the two computations. Figs. 4a and 5a show that at equilibrium if $Y/\rho_o = -10$ and $\rho_o = 1$, in the non-ideal case ρ_{Cl^-}/ρ_o has a higher value than in the ideal case and that the value of $\rho_{Ca^{2+}}/\rho_o$ is not sensitive to the non-ideal assumptions. Therefore the current should be higher in the non-ideal case than in the ideal one. The numerical results show that the anionic flux is higher in the non-ideal case than in the ideal one as it should be. But the cationic flux is a little smaller in the non-ideal case. The lower value of cationic current density balances the higher value of the anionic one because the cationic one is the main contribution to I_C. As Y/ρ_o decreases, the non-ideal density profiles must approach the ideal ones because the densities decrease in the membrane. Therefore all the non-ideal current/voltage curves must be close to the ideal ones.

We can deduce also that the I_L value must be identical in the two hypotheses. However the estimated value cannot be accurate because the value of the flux ratio $|J_{Ca^{2+}}/J_{Cl^-}|$ is close to unity owing to the high value of ρ_{Cl^-}/ρ_o in the membrane at equilibrium. If $Y/\rho_o = -10$ and $\rho_o = 1$, in the ideal case $I_L = 3.9I_{LO}$ and in the non-ideal case $I_L = 5.4I_{LO}$. As Y/ρ_o approaches 2, the flux ratio approaches unity and I_L approaches $10I_{LO}$ and $12I_{LO}$ in the ideal and non-ideal case.

In Fig. 6b the current/voltage curves for the two electrolytes with $Y/\rho_o = -10$ and with ρ_o ranging from 0.01 to 1 are displayed. For the two electrolytes at a given value of $\Delta\Phi$, the current density increases with ρ_o if $\rho_o \leq 0.1$ and decreases as ρ_o increases from 0.1 to 1. This variation is correlated to the variation of anion density ratio in the membrane at equilibrium (see Figs. B4a and 5a). In the case of NaCl, if $\rho_o \leq 0.1$, ρ_{Cl^-}/ρ_o increases slightly with ρ_o, i.e. its value is a little greater than the value computed with the ideal assumption, and ρ_{Na^+}/ρ_o remains constant. Therefore the non-ideal curves are above but close to the ideal one. But if $\rho_o > 0.1$, ρ_{Cl^-}/ρ_odrops abruptly inducing a high decrease of the ionic flux of the two species. In the case of $CaCl_2$, the variation of ρ_{Cl^-}/ρ_o with ρ_o (Fig. 5a) is more important if $\rho_o \leq 0.1$ and the value of ρ_{Cl^-}/ρ_o is much higher than in the ideal case. At a given value of $\Delta\Phi$, the variation of $J_{Ca^{2+}}$ and of J_{Cl^-} with ρ_o follows the variation of ρ_{Cl^-}/ρ_o and these fluxes are higher than the ideal ones when $\rho_o \leq 0.1$. However the computations carried out at equilibrium with $\rho_o = 0.01$ and $\rho_o = 1$ lead to the same density ratio for the two species inside the membrane. At a given value of $\Delta\Phi$, the minimum values of ρ_{Cl^-}/ρ_o inside the membrane are comparable for the two salt densities ρ_o (e.g. when $\chi\Delta\Phi = -8.4$, $\rho_{Cl^-}/\rho_o = 0.39$, 0.524, 0.33 if $\rho_o = 0.01$, 0.1, 1 respectively). But at this electric potential drop $J_{Ca^{2+}}(r_o = 1) = 0.92J_{Ca^{2+}}(\rho_o = 0.01)$ and $J_{Cl^-}(r_o = 1) = 0.94J_{Cl^-}(r_o = 0.01)$. So the difference between the two current/voltage curves when $\rho_o = 0.01$ and $\rho_o = 1$ cannot be explained by the density profiles. The magnitude of non-ideal effects is much smaller if $\rho_o = 0.01$ than if $\rho_o = 1$. May be that the non-ideal contribution influences the density profiles and also the current density directly by decreasing the ionic fluxes.

5. Conclusion

The density and the potential distribution have been studied in a membrane system constituted of a negatively charged membrane separating two baths. A wide range of salt density and of membrane charge has been investigated in order to study the non-ideal effects on the equilibrium and on the ionic transport induced by an electric potential drop. Non-ideal contribution has been taken into account by means of the DFT in order to extend the Nernst–Planck equation. The symmetric electrolyte NaCl and the unsymmetric one $CaCl_2$ have been used in this investigation.

At equilibrium, the numerical results have shown that the whole charge discontinuity on both sides of the bath/membrane interfaces decreases and the electric potential in the membrane increases with the increasing salt density (ρ_o). In the case of the unsymmetric electrolyte and at high values of ρ_o, ionic secondary layers have been observed with a charge inversion on both sides of the bath/membrane interfaces and with a positive value of the membrane electric potential. As the salt density increases to 0.1, the co-ion density ratio inside the membrane increases and then decreases as ρ_o increases from 0.1 to 1. But the counter-ion density ratio is not sensitive to the salt density. In the membrane, the analysis of the contribution of each individual chemical potential component has been carried out. For the two electrolytes the counter-ion density ratio is controlled by the balance between the increase of the es component and the decrease of the electric potential one. For the co-ion, as long as $\rho_o < 0.1$, the density ratio is controlled by the electric potential component which is less and less repulsive as ρ_o increases. In the range $\rho_o > 0.1$, the magnitude of the *es* component increases with ρ_o and becomes comparable to the electric potential one. The *es* contribution is less and less attractive and induces a decrease of the density ratio as ρ_o increases.

If a negative electric potential drop is imposed, the charge distribution is modified outside the membrane. The thickness of the EDL on the left side increases as observed in the case of the ideal assumption. The position of the secondary layers is not sensitive to the electric potential drop. However the amplitude of these layers in the left bath decreases and it increases a little in the right bath. Concerning the current/potential curves, the difference between the ideal curves and the non-ideal ones are correlated to the co-ion density ratio ρ_{Cl^-}/ρ_o in the membrane computed at equilibrium in the non-ideal case. Therefore the non-ideal curves position with respect to the ideal one depends on the value of ρ_o. For a given value of ρ_o, the difference between the ideal curves and the non-ideal ones decreases with Y because the ion densities and the non-ideal contributions decrease with Y.

Nomenclature

C^{es}	short range of the electrostatic pair correlation
D_i	diffusion coefficient of species i
e	elementary charge
F	Helmoltz free energy
I	ionic strength
I_C	current density
I_L	limiting current density of the membrane
I_{LO}	limiting current density of a perfectly permselective membrane
J_i	flux density of species i
k	Boltzmann constant
L	membrane thickness
$n^{(\alpha)}$	weighted function
Q	local charge
Q_{out}	whole charge ratio in the outer electric double layer
R_i	ionic radius of species i
R_f	mean radius of the reference fluid
T	absolute temperature

V_{ext}	external potential
W, $W^{(\alpha)}$	weight functions, α=0,1,2,3,ν1,ν2
x	longitudinal direction
Y	fixed charge inside the membrane
z_i	electric charge of species i

Greek letters

δ	thickness of the right and left bath
ε	relative constant dielectric of the solvent
Γ	MSA screening length
λ_d	Debye length
λ_i	capacitance length of species i
Λ_i	de Broglie thermal wavelength of species i
μ_i	chemical potential of species i
μ_i^{ε}	contribution of component ε to chemical potential of species i, ε=hs, es, Φ, ρ
v_i	valence of species i
Φ	electric potential
Φ_d	Donnan electric potential
$\Phi_{1/2}$	electric potential at the membrane centre
ρ_o, ρ_{oi}	density of electrolyte and of species i at $x=-\delta$
ρ_i, ρ_i^{ref}	density of species i in the membrane system and in the reference fluid
Ω	grand thermodynamic potential

Appendix A

The DFT describes the thermodynamic equilibrium of inhomogeneous systems, of volume V and submitted to an external potential $V_{ext}(\vec{r})$, in contact with a reservoir characterised by a temperature T and a chemical potential μ [21,22]. At equilibrium, the temperature and the chemical potential of these systems must be equal to those of the reservoir. In the case of ionic fluids, the electrolyte is assumed to be a mixture of species i which are hard sphere of radius R_i and of charge number z_i. The species are immersed in a solvent which is a dielectric continuum. The equilibrium distribution of density is obtained by minimisation of the grand canonical potential Ω with respect to the species density $\rho_i(\vec{r})$:

$$\frac{\delta\Omega\left[\rho_i(\vec{r})\right]}{\delta\rho_i(\vec{r})}=\frac{\delta}{\delta\rho_i(\vec{r})}\left(F\left[\rho_i(\vec{r})\right]+\sum_{ij}\int d\vec{r}'\rho_i(\vec{r}')\left[V_{ext}(\vec{r}')-\mu_i\right]\right)=0 \tag{A.1}$$

Ω is expressed as a functional of the local density $\rho_i(\vec{r})$, $\rho_i(\vec{r})$ is the density of the species i located at $\vec{r}$, F is the Helmholtz free energy, $V_{ext}(\vec{r})$ is a non-electrostatic external potential and μ_i is the chemical potential of species i. $\delta/\delta\rho_i(\vec{r})$ means the functional derivative. The Helmholtz free energy F is decomposed into two terms: the ideal one F^{id} and the excess one F^{ex}. The excess term comes from the interactions between ions. These interactions are of two kinds: the short range hard sphere (hs) interaction and the long range electrostatic (es) one. F^{ex} is divided into the two corresponding terms F^{hs} and F^{es}.

Using the complete expression of the grand canonical potential, the chemical potential has the following expression in the one dimension formulation:

$$\begin{aligned}\mu_i(x)&=\frac{\delta F^{id}\left[\rho_j(x')\right]}{\delta\rho_i(x)}+\frac{\delta F^{hs}\left[\rho_j(x')\right]}{\delta\rho_i(x)}+\frac{\delta F^{es}\left[\rho_j(x')\right]}{\delta\rho_i(x)}\\&=\mu_i^{id}(x)+\mu_i^{hs}(x)+\mu_i^{es}(x)\end{aligned} \tag{A.2}$$

The ideal chemical potential expression is

$$\mu_i^{id}(x)=kT\,Ln\rho_i(x)\Lambda_i^3+z_ie\Phi(x) \tag{A.3}$$

where $\Phi(x)$ is the local electric potential related to the ion density by means of the Poisson equation:

$$\varepsilon\frac{\partial^2}{\partial x^2}\Phi(x)=-e\sum_i z_i\rho_i(x) \tag{A.4}$$

e is the elementary charge and $\mu_i^{id}(x)$ is in fact the classical electrochemical potential. In the case of charged membrane, the electric potential created by external charges, i.e. the fixed charges of the membrane, is included in the electric potential Φ. So in Eq. (A.4) the fixed charge density Y must be added. In the following these charges do not contribute to the excess free energy because they are assimilated to points.

To express the hard sphere component, the fundamental measure theory is applied and μ^{hs} takes the form [43]:

$$\mu_i^{hs}(x)=kT\sum_{\alpha}\int_{x-R_i}^{x+R_i}dx'\frac{\partial}{\partial n_\alpha}f^{hs}(\{n_\alpha(x')\})W_i^{(\alpha)}(x-x') \tag{A.5}$$

With

$$\begin{aligned}f^{hs}(\{n_\alpha(x')\})=&-n_0Ln(1-n_3)+\frac{n_1n_2-n_{V1}n_{V2}}{1-n_3}\\&+\frac{n_2^3}{24\pi(1-n_3)^2}\left(1-\frac{n_{V2}n_{V2}}{n_2^2}\right)^3\end{aligned} \tag{A.6}$$

$$n_\alpha(x)=\sum_i\int_{x-R_i}^{x+R_i}dx'\rho_i(x)W_i^{(\alpha)}(x-x') \tag{A.7}$$

$n_\alpha(x)$ are the 6 non-local densities and $W_i^{(\alpha)}(x)$ are the corresponding weight functions given in [38,43]:

$$4\pi R_i^2W_i^{(0)}(x)=4\pi R_iW_i^{(1)}(x)=W_i^{(2)}(x)=2\pi R_i \tag{A.8a}$$

$$W_i^{(3)}(x)=\pi(R_i^2-x^2) \tag{A.8b}$$

$$4\pi R_i^2W_i^{(V1)}(x)=W_i^{(V2)}(x)=2\pi xe_x \tag{A.8c}$$

The weight functions are characteristics of the particle geometry. The scalar functions $W_i^{(2)}(\vec{r})$ and $W_i^{(3)}(\vec{r})$ are related to the surface area and the volume of the spherical particle respectively. The surface vector function $W_i^{(V2)}(\vec{r})$ characterises the variance across the particle surface. In three dimension, the other weight functions are proportional to the function $W_i^{(2)}$ and $W_i^{(V2)}$. The weight functions are chosen from the convolution decomposition of the pair exclusion between two spheres of radii R_i and R_j: $\theta(R_i-R_j-|\vec{r}-\vec{r}'|)$ which represents the Mayer function for a mixture of hard spheres in the limit of small particle density. Eq. (8) represents these weight functions integrated in two directions.

The electrostatic component of the Helmholtz free energy is expressed by means of a second order Taylor expansion with respect to a homogeneous fluid named also reference fluid [43]. The functional derivative with respect to the density gives the following one-dimensional expression of the es chemical potential:

$$\mu_i^{es}(x)=\mu_i^{es}[\rho_i^{ref}]-kT\sum_j\int_{x-R_i}^{x+R_i}dx'C_{ij}^{es}(x,x')\Delta\rho_j(x') \tag{A.9}$$

where $C_{ij}^{es}[x,x']$ is the short range electrostatic part of the two particle direct correlation of the reference fluid [44], $\Delta\rho_i(x)=\rho_i(x)-\rho_i^{ref}$ and ρ_i^{ref} is the density of the species i in the reference fluid. The long range part of the direct correlation is included in electric potential Φ. The reference fluid must be charge neutral and is in our case the electrolytic fluid far away from the membrane. It is convenient to use the primitive

version of the MSA theory because of the analytical expression of C_{ij}^{es}, of $\mu_i^{es}[\rho_i^{ref}]$ and of the screen parameter Γ [45].

$$C_{ij}^{es}(x,x') = -\frac{z_i z_j e^2}{8\pi\varepsilon}\frac{1}{\lambda_i\lambda_j}\left[\frac{1}{3}(R_{ij}^3 - |x-x'|^3) - \lambda_{ij}(R_{ij}^2 - |x-x'|^2) + \lambda_{ij}^2(R_{ij} - |x-x'|)\right]$$
$$\text{if} \quad |x-x'| \le R_i + R_j$$

$$C_{ij}^{es}(x,x') = 0 \text{ if } |x-x'| > R_i + R_j \tag{A.10}$$

$$R_{ij} = R_i + R_j, \quad \lambda_{ij} = \lambda_i + \lambda_j, \text{ and } \lambda_i = R_i + \frac{1}{2\Gamma(x)} \tag{A.11}$$

Γ, which is the MSA version of the inverse of the screening length, is given by the following expression:

$$4\Gamma^2 = \frac{e^2}{kT\varepsilon\varepsilon_o}\sum_i \rho_i\left[\frac{z_i - 4\eta R_i^2}{1+2\Gamma R_i}\right]^2 \tag{A.12}$$

With

$$\eta = \frac{1}{\Omega}\frac{\pi}{2\Delta}\sum_j \frac{2\rho_j R_j z_j}{1+2\Gamma R_j} \tag{A.13a}$$

$$\Omega = 1 + \frac{\pi}{2\Delta}\sum_j \frac{8\rho_j R_j^3}{1+2\Gamma R_j} \tag{A.13b}$$

$$\Delta = 1 - \frac{\pi}{6}\sum_j 8\rho_j R_j^3 \tag{A.13c}$$

However, the perturbational approach with respect to the reference fluid can be used only if the local density does not vary in large amounts. In order to circumvent this problem, an alternative was proposed [38,39]. It consists in determining a local reference fluid which is electroneutral and which has the same ionic strength as the local fluid. In order to avoid discontinuity, ρ_i^{ref} is a density averaged over a sphere of radius R_f. In one dimension:

$$\rho_i^{ref}(x) = \int dx' \overline{\rho}_i(x') W(x,x') \tag{A.14}$$

where $\overline{\rho}_i(x)$ satisfies the electroneutrality and the ionic strength conditions mentioned above. The expression of $W(x,x')$ and of R_f are:

$$W(x,x') = \frac{\pi(R_f^2(x) - |x-x'|^2)}{(4\pi/3)R_f^3(x)} \tag{A.15}$$

$$R_f(x) = \frac{\sum_i \overline{\rho}_i(x) R_i}{\sum_i \overline{\rho}_i(x)} + \frac{1}{2\Gamma(x)} \tag{A.16}$$

Agreement with Monte Carlo results in the case of the computation of the electric double layer against a charged plane [40,46] and the agreement with experimental data in the case of ion transport through ion channel [47] have proved the accuracy of the local reference fluid concept.

Appendix B

Figs. B1 and 2 display, on both sides of the left bath/membrane interface, the profiles of the density ratios ρ_i/ρ_o, of the electric potential and of the local charge density ratio Q/ρ_o in the case of the symmetric electrolyte NaCl. These profiles are computed with $Y/\rho_o = -10$ and for ρ_o varying from 10^{-4} to 1. Q is defined as $Q = \rho_{Na^+} - \rho_{Cl^-} + Y$. Inside the cationic density boundary layer ρ_{Na^+}/ρ_o decreases slightly in the bath side and increases in the membrane side as ρ_o increases. However the density at the centre

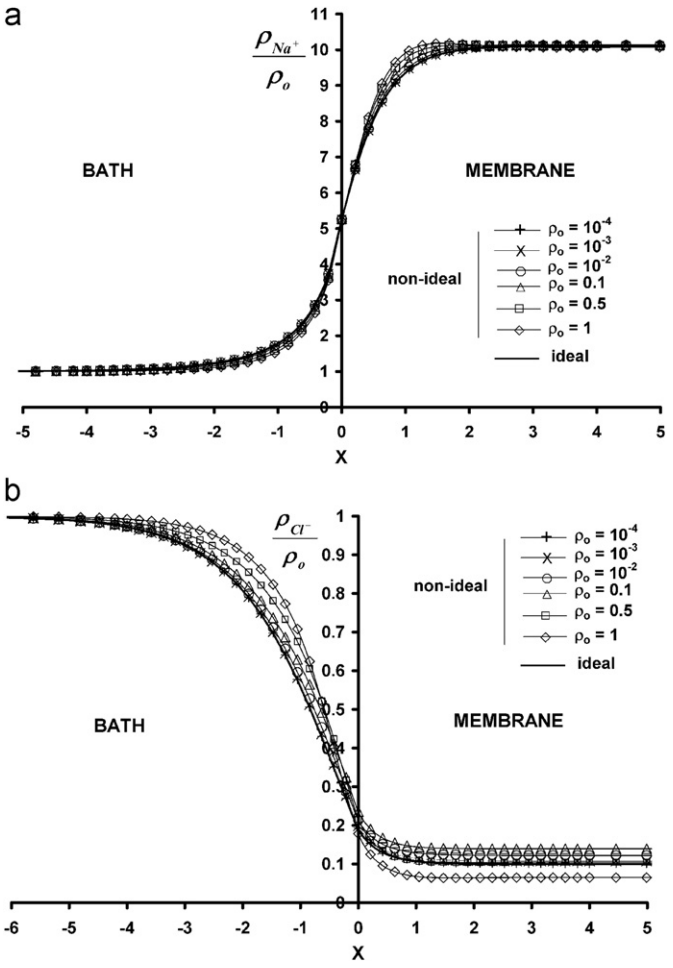

Fig. B1. : Electrolyte: NaCl. Ion density ratio profiles on both sides of the left bath/membrane interface at equilibrium for several salt density values. $Y/\rho_o = -10$.

of the membrane remains invariant. The difference between the ideal curve and the non-ideal ones is noticeable when $\rho_o > 0.1$ inside the membrane. At the same time a local maximum of small magnitude appears inside the membrane at $x = 1.5$. The profiles of Cl^- are much more sensitive to ρ_o. In the bath, we can observe a salt density threshold value of 0.1 over which the density ratio ρ_{Cl^-}/ρ_o increases with ρ_o. In the membrane the salt density threshold value is 0.01. As ρ_o increases to 0.1, ρ_{Cl^-}/ρ_o increases to a value of 0.139 at the membrane centre and ρ_{Cl^-}/ρ_o decreases to 0.065 when ρ_o increases from 0.1 to 1. Concerning the electric potential (Fig. B2a), outside the membrane, the value of the salt density threshold is close to 0.01. Inside the membrane, the threshold value is 10^{-3}. As ρ_o increases from 10^{-4} to 1 the electric potential at the membrane centre increases from -1 to -0.48. At the same time the potential boundary layer thickness decreases from 2 to 1. As for $CaCl_2$, outside the membrane the whole charge ratio in the EDL decreases if the value of ρ_o is greater than the threshold value of around 0.01 (Fig. B2b). When $\rho_o = 1$, a maximum with a positive value appears at $x = 1.5$, corresponding to the maximum observed in the cation profiles.

Figs. B3 and 4 show the variation of $\Delta\mu_i^{\varepsilon}$ with ρ_o as Figs. 4 and 5. Strong similarities can be observed between these two sets of figures. Fig. B3 shows that the density ratio ρ_{Na^+}/ρ_o depends on two contributions: the electric potential component ($\Delta\mu_{Na^+}^{\varphi}$) and the electrostatic one ($\Delta\mu_{Na^+}^{es}$) over all the salt density range. The density ratio is independent of ρ_o. This means that the increase of

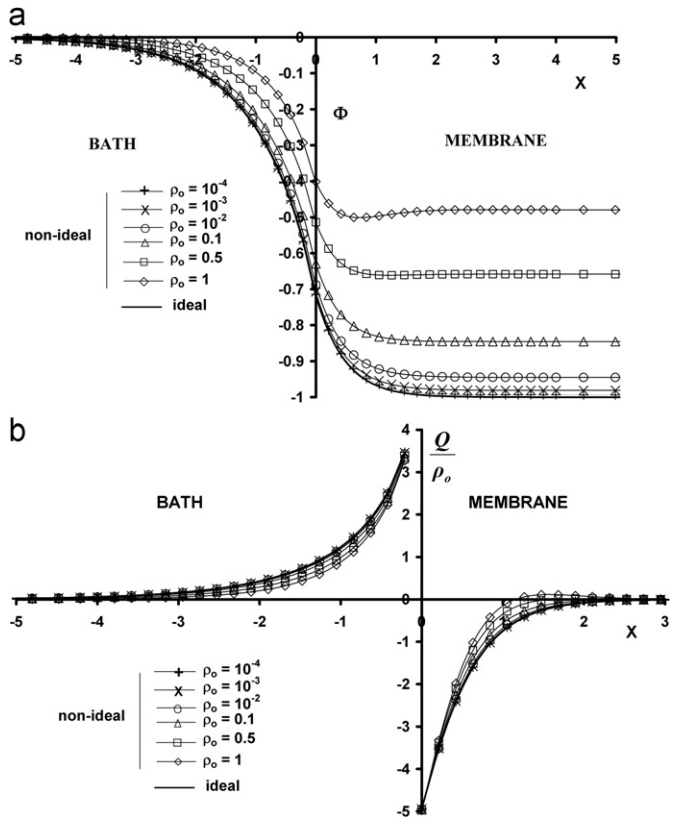

Fig. B2. : Electrolyte: NaCl. Electric potential and charge density ratio profiles on both sides of the left bath/membrane interface at equilibrium for several salt density values. $Y/\rho_o = -10$.

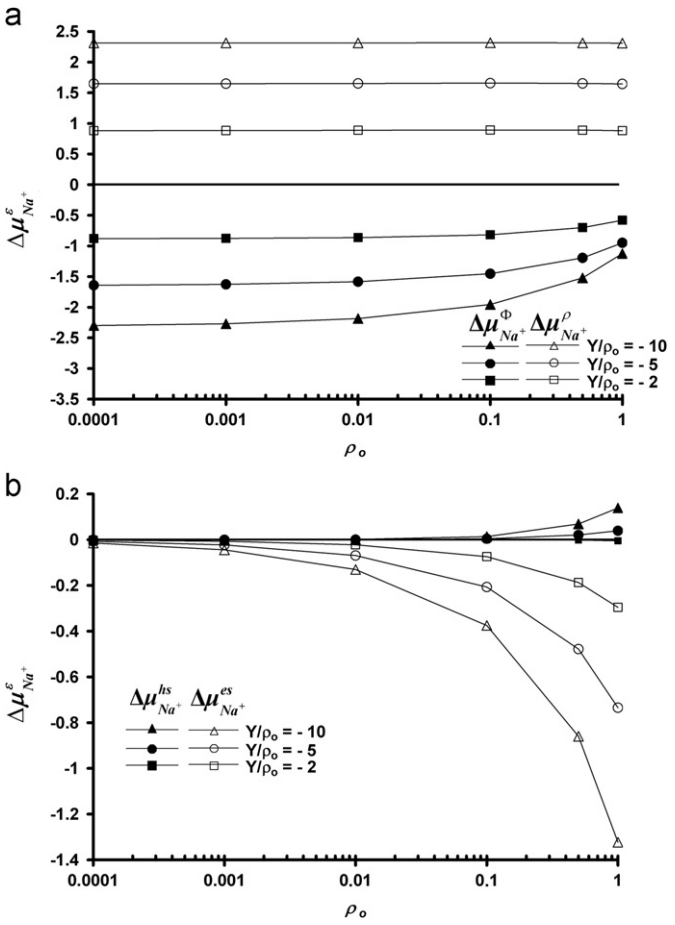

Fig. B3. Electrolyte: NaCl. Species: Na^+. Difference of each chemical potential contribution between the membrane centre and the left boundary vs. the salt density for several values of the membrane charge density ratio Y/ρ_o. (a) Density and electric potential contribution and (b) electrostatic and hard sphere contribution.

$\Delta\mu^{\varphi}_{Na^+}$ balances the decrease of $\Delta\mu^{es}_{Na^+}$. The rate of variation is noticeable when $\rho_o > 0.01$. As observed for $CaCl_2$, $\Delta\mu^{es}_i$ depends on the screening ability of each species at these two locations separately $x = -\delta$ and $x = L/2$. This explains the variation of $\Delta\mu^{es}_{Na^+}$ without any noticeable variation of $\Delta\mu^{\rho}_{Na^+}$. For the co-ion (Fig. B4b), $\Delta\mu^{es}_{Cl^-}$ and $\Delta\mu^{hs}_{Cl^-}$ must be taken into account if $\rho_o > 0.1$whatever the value of Y/ρ_o. So, when $\rho_o < 0.1$, the increase of ρ_{Cl^-}/ρ_o with ρ_o is mostly controlled by the electric potential contribution which is less and less repulsive. If $\rho_o > 0.1$, the decrease of the density ratio corresponds to the increase of $\Delta\mu^{es}_{Cl^-}$ and of $\Delta\mu^{hs}_{Cl^-}$ which are repulsive in this range of ρ_o. This means that ρ_{Cl^-}/ρ_o has a maximum located around $\rho_o = 0.1$ as observed in Fig. B1b.

Appendix C

Here are described the profiles of density, of potential and of local charge of an unsymmetric electrolyte under an electric potential drop. In Fig. C1 are shown the profiles of the electric potential, of the density ratios $\rho_{Ca^{2+}}/\rho_o$ and ρ_{Cl^-}/ρ_o and of the charge density ratio Q/ρ_o with the following set of parameter values: $\rho_o = 1$, $Y = -10$ and $\Delta\Phi = \Phi(\delta + L) = 0$, -5 and -10 ($I_C = 0$, $1.73 I_{LO}$ and $2.9 I_{LO}$ respectively).

In Fig. C1a, the electric potential profiles computed with ideal and non-ideal approximation are compared. At the membrane centre the electric potential difference between the two kinds of computation is independent of $\Delta\Phi$. As the electric potential drop increases, the electric potential decreases less and less linearly in the two baths, revealing that the current density tends to the limiting one I_L. However, it was observed that even at moderate potential drop ($\Delta\Phi = -1.5$, $I_C = 0.55 I_{LO}$) the decrease is not linear in the left bath if the non-ideal hypothesis is used. This was not observed with the ideal approximation.

If the electrolyte is NaCl, in the three regions where the electroneutrality condition occurs, the linear variation of ρ_{Cl^-}/ρ_o and of ρ_{Na^+}/ρ_o was observed over all the potential drop range investigated with the ideal hypothesis and the non-ideal one. Dividing the N.P. equation in the ideal form by D_i and summing over the species, we find:

$$-\sum_i \frac{J_i}{D_i} = \sum_i \frac{\partial}{\partial x}\rho_i + z_i \rho_i \chi \frac{\partial}{\partial x}\Phi \tag{C.1}$$

Using the electroneutrality condition $\sum_i z_i \rho_i + Y = 0$, we obtain the following relation:

$$\sum_i \frac{\partial}{\partial x}\rho_i = -\sum_i \frac{J_i}{D_i} + \chi Y \frac{\partial}{\partial x}\Phi \tag{C.2}$$

Integrating over a region $[x_o, x]$ where Y and $(\partial/\partial x)\Phi$ are constant, the density of each species follows the linear relation:

$$\rho_1(x) = \rho_1(x_o) + \frac{z_2}{z_2 - z_1}\left(\chi Y \frac{\partial}{\partial x}\Phi - \sum_i \frac{J_i}{D_i}\right)(x - x_o) \tag{C.3}$$

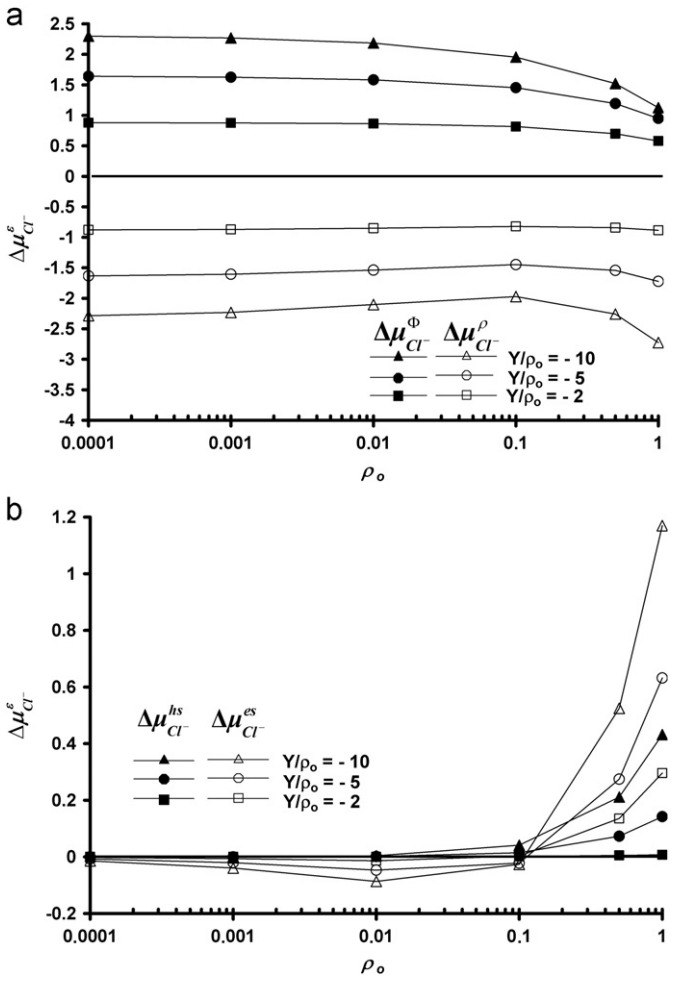

Fig. B4. Electrolyte: NaCl. Species: Cl^-. Difference of each chemical potential contribution between the membrane centre and the left boundary vs. the salt density for several values of the membrane charge density ratio Y/ρ_o. (a) Density and electric potential contribution and (b) electrostatic and hard sphere contribution.

$$\rho_2(x) = \rho_2(x_o) + \frac{z_1}{z_1 - z_2}\left(\chi Y \frac{\partial}{\partial x}\Phi - \sum_i \frac{J_i}{D_i}\right)(x - x_o) \qquad (C.4)$$

If the electrolyte is symmetric, the DFT simulations give a slope equal to 1/2 for the two species ($z_2/z_2 - z_1 = z_1/z_1 - z_2 = 1/2$) even in the membrane where the electroneutrality condition is verified. So the non-ideality effects on the linear variation are not observed in the present work.

This is not the case of $CaCl_2$ in Fig. C1b. In this figure, the density ratio profiles show that the longitudinal position of the extrema remains at the same place. Even if $I_C \gg I_{LO}$, the co-ion density ratio near the left bath/membrane interface is not close to zero because the value of ρ_{Cl^-}/ρ_o in the membrane at equilibrium is close to ν_{Cl^-}. In the regions where the electroneutrality condition occurs the densities do not vary linearly. This non-linearity increases with $\Delta\Phi$. However in these regions if the profiles are approximated to straight lines, the slope of $\rho_{Ca^{2+}}/\rho_o$ curve is twice the slope of ρ_{Cl^-}/ρ_o curve as predicted by Eqs. (C.3) and (C.4).

Fig. C1c shows that the structure of the EDL is independent of $\Delta\Phi$. Inside the membrane, the position and the magnitude of the extrema does not change significantly. In the left bath, the magnitude of the minimum decreases and its local position moves away from the interface. The thickness of the negative

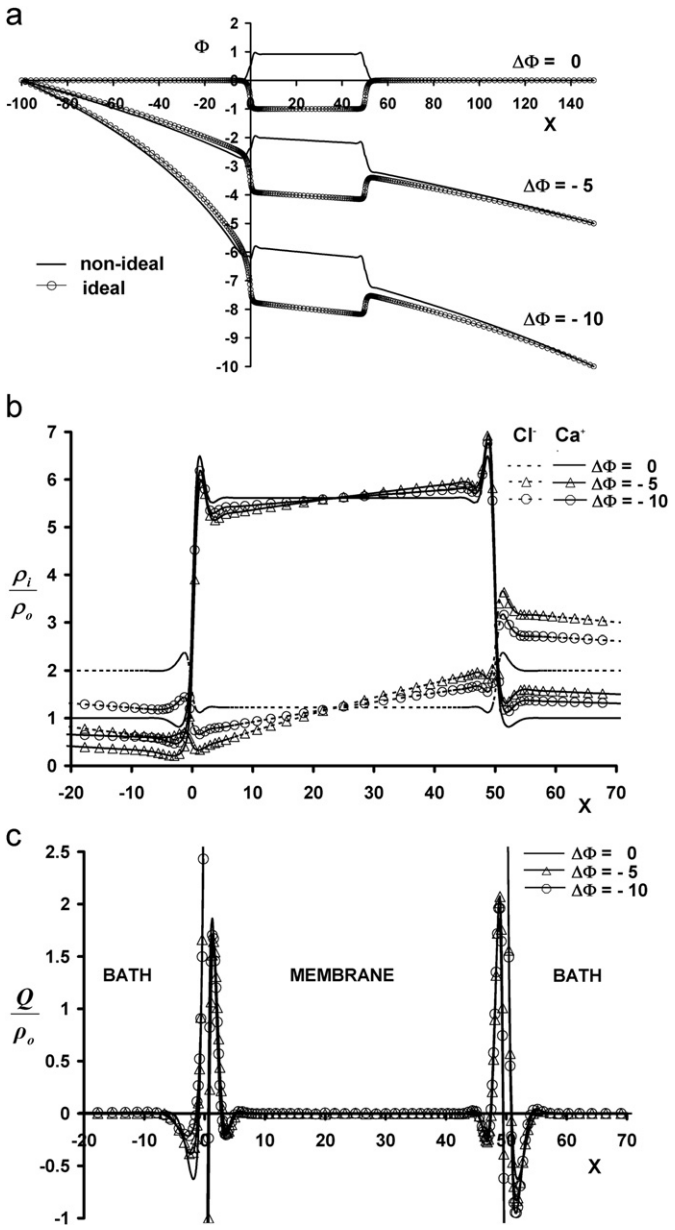

Fig. C1. : Electrolyte: $CaCl_2$. Longitudinal profiles for several potential drop values. $\rho_o = 1$, $Y/\rho_o = -10$: (a) ion density ratios; (b) electric potential and (c) charge density ratio.

charge secondary layer increases as I_C tends to I_L. The whole charge ratio of the outer EDL in the left bath is less and less negative contrary to the whole one in the right bath. However the computational domain remains electroneutral.

References

[1] R.P. Buck, Kinetics of bulk and interfacial ionic motion: microscopic bases and limits for the Nernst–Planck equation applied to membrane systems, J. Membr. Sci. 17 (1984) 1–62.

[2] A.E. Yaroshchuk, Dielectric exclusion of ions from membranes, Adv. Colloid Interface Sci. 85 (2000) 195–230.

[3] R. Yamamoto, H. Matsumoto, A. Tanioka, Ionic transport behavior across charged membranes with low water content. I. Theoretical aspect of membrane potentials in membranes having inhomogeneously distributed fixed-charge groups, J. Chem. Phys. B 107 (2003) 10615–10622.

[4] E.C. Cwirko, R.G. Carbonell, Interpretation of transport coefficients in Nafion using a parallel pore model, J. Membr. Sci. 67 (1992) 227–247.

[5] J. Cervera, V. Garcia-Morales, J. Pellicer, Ion size effect on the electrokinetic flow in nanoporous membranes caused by concentration gradients, J. Phys. Chem. B 107 (2003) 8300–8309.
[6] A.T. Bosch, Analytical theory for permeation of condensable gases in a nanopore, J. Membr. Sci. 323 (2008) 271–277.
[7] Y. Liu, M. Liu, W.M. Lau, J. Yang, Ion size and image effect on electrokinetic flows, Langmuir 24 (2008) 2884–2891.
[8] Y. Luo, E. Harder, R.S. Faibish, B. Roux, Computer simulations of water flux and salt permeability of the reverse osmosis FT-30 aromatic polyamide membrane, J. Membr. Sci. 384 (2011) 1–9.
[9] Zhen Yang, Xiaoning Yang, Zhijun Xu, Structure of hard-core Yukawa fluid mixtures near a semi-permeable membrane: a density functional study, J. Membr. Sci. 320 (2008) 381–389.
[10] A. Lehmani, O. Bernard, P. Turq, Transport of ion and solvent in confined media, J. Stat. Phys. 89 (1997) 379–402.
[11] Y. He, D. Gillespie, D. Boda, I. Vlassiouk, R.S. Eisenberg, Z.S. Siwy, Tuning transport properties of nanofluidic devices with local charge inversion, J. Am. Chem. Soc. 131 (2009) 5194–5202.
[12] R.B. Schoch, J. Han, P. Renaud, Transport phenomena in nanofluids, Rev. Mod. Phys. 80 (2008) 839–883.
[13] J. Cervera, P. Ramirez, J.A. Manzanares, S. Mafé, Incorporating ionic size in the transport equations for charged nanopores, Microfluid Nanofluid 9 (2010) 41–53.
[14] J.J. Lopez-Garcıa, M.J. Aranda-Rascon, C. Grosse, J. Horno, Equilibrium electric double layer of charged spherical colloidal particles: effect of different distances of minimum ion approach to the particle surface, J. Phys. Chem. B 114 (2010) 7548–7556.
[15] D. Gillespie, A.S. Khair, J.P. Bardhan, S. Pennathur, Efficiently accounting for ion correlations in electrokinetic nanofluidic devices using density functional theory, J. Colloid Interface Sci. 359 (2011) 520–529.
[16] M.Z. Bazant, M.S. Kilic, B.D. Storey, A. Adjari, Towards an understanding of induced-charge electrokinetics at large applied voltages in concentrated solutions, Adv. Colloid Interface Sci. 152 (2009) 48–88.
[17] M. Lozada-Cassou, D. Henderson, Application of the hypernetted chain approximation to the electrical double layer. Comparison with Monte-Carlo results for 2:1 and 1:2 salts, J. Phys. Chem. 87 (1983) 2821–2824.
[18] L.B. Bhuiyana, C.W. Outhwaite, Comparison of the modified Poisson–Boltzmann theory with recent density functional theory and simulation results in the planar electric double layer, Phys. Chem. Chem. Phys. 6 (2004) 3467–3472.
[19] K. Wang, Y.X. Yu, G.H. Gao, Density functional study on the structure and thermodynamic properties of small ions around polyanionic DNA, Phys. Rev. E 70 (2004) 011912.
[20] M. Valisko, D. Boda, D. Gillespie, Selective adsorption of ions with different diameter and valence at highly charged interfaces, J. Phys. Chem. C 111 (2007) 15575–15585.
[21] R. Evans, The nature of the liquid–vapour interface and other topics in statistical mechanics of non-uniform, classical fluids, Adv. Phys. 28 (1979) 143–200.
[22] J.P. Hansen, I.R. Mc-Donald, Theory of Simple Liquids, 2nd ed., Academic Press, 1986.
[23] J. Wu, Density functional theory for chemical engineering: from capillarity to soft materials, AIChE J. 52 (2006) 1169–1193.
[24] D. Gillespie, L. Xu, Y. Wang, G. Meissner, (De)constructing the ryanodine receptor: modeling ion permeation and selectivity of the calcium release channel, J. Phys. Chem. B 109 (2005) 15598–15610.
[25] V.M. Volgin, A.D. Davidov, Ion transport through ion-exchange and bipolar membranes, J. Membr. Sci. 259 (2005) 110–121.
[26] V.V. Nikonenko, N.D. Pismenskaya, E.I. Belova, P. Sistat, P. Huguet, G. Pourcelly, C. Larchet, Intensive current transfer in membrane systems: modelling, mechanism and application in electrodialysis, Adv. Colloid Interface Sci. 160 (2010) 101–123.
[27] J.A. Manzanares, W.D. Murphy, S. Mafé, H. Reiss, Numerical simulation of the nonequilibrium diffuse double layer in ion-exchange membranes, J. Phys. Chem. 97 (1993) 8524–8530.
[28] A.A. Moya, J. Horno, Application of the network simulation method to ionic transport in ion-exchange membrane including diffusion double-layer effects, J, Phys. Chem. B 103 (1999) 10791–10799.
[29] Y. Yang, P.N. Pintauro, Multicomponent space-charge transport model for ion-exchange membranes, AIChE J. 46 (2000) 1177–1190.
[30] R. Chien, H. Chen, C. Liao, Investigation of ion concentration and electric potential distributions in charged membrane/electrolyte systems, J. Membr. Sci. 342 (2008) 121–130.
[31] X.L. Wang, T. Tsuru, S. Nakao, S. Kimura, Electrolyte transport through nanofiltration membranes by the space-charge model and the comparison with Toerell–Meyer–Sievers model, J. Membr. Sci. 103 (1995) 117–133.
[32] X. Lefebvre, J. Palmeri, P. David, Nanofiltration theory: an analytic approach for single salts, J. Phys. Chem. B 108 (2004) 16811–16824.
[33] J.-F. Dufrêche, O. Bernard, S. Durand-Vidal, P. Turq, Analytical Theories of transport in concentrated electrolyte solutions from the MSA, J. Phys. Chem. B 109 (2005) 9873–9884.
[34] P. Wang, A. Anderko, Computation of dielectric constants of solvent mixtures and electrolyte solutions, Fluid Phase Equilibria 186 (2001) 103–122.
[35] U. Marconi, P. Tarazona, Dynamic density functional theory of fluids, J. Chem. Phys. 110 (1999) 8032–8044.
[36] L.J.D. Frink, A. Thomson, A. Salinger, Applying molecular theory to steady-state diffusing systems, J. Chem. Phys. 112 (2000) 7564–7571.
[37] A.J. Archer, Dynamic density functional theory for dense atomic liquids, J. Phys. Condens. Matter 18 (2006) 5617–5628.
[38] D. Gillespie, W. Nonner, R.S. Eisenberg, Coupling Poisson–Nernst–Planck and density functional theory to calculate ion flux, J. Phys. Condens. Matter 14 (2002) 12129–12145.
[39] D. Gillespie, W. Nonner, R.S. Eisenberg, Density functional theory of charged, hard sphere fluids, Phys. Rev. E 68 (2003) 031503.
[40] D. Gillespie, M. Valisko, D. Boda, Density functional theory of the electrical double layer: the RFD functional, J. Phys. Condens. Matter 17 (2005) 6609–6626.
[41] V.G. Levich, Physicochemical Hydrodynamics, Prentice-Hall, Englewood Cliffs, NJ, 1962.
[42] J.A. Manzanares, K. Kontturi, Diffusion and migration, in: A.J. Bard (Ed.), Encyclopedia of Electrochemistry, vol. 2, Wiley-VCH, 2003, pp. 81–145.
[43] Y. Rosenfeld, Free energy model for inhomogeneous fluid mixtures: Yukawa-charged hard spheres, general interaction, and plasmas, J. Chem. Phys. 98 (1993) 8126–8148.
[44] L. Blum, Y. Rosenfeld, Relation between the free energy and the direct correlation function in the mean spherical approximation, J. Stat. Phys. 63 (1991) 1177–1190.
[45] S. Durand-Vidal, J.P. Simonin, P. Turk, Electrolytes at Interfaces (Progress in Theoretical Chemistry and Physics), Kluwer Academic Publishers, 2002.
[46] J. Reszko-Zygmunt, S. Sokolowski, Application of a density functional approach to nonuniform ionic fluids: the effect of association, Condens. Matter Phys. 7 (2004) 793–804.
[47] D. Gillespie, J. Gin, M. Fill, Reinterpreting the anomalous mole fraction effect: the Ryanodine receptor case study, Biophys. J. 97 (2009) 2212–2221.